CHEMISTRY OF MATERIALS

Article

pubs.acs.org/cm

Spin-Glass Behavior in Graphene Oxide Powders Induced by Nonmagnetic Sodium Sulfate

Dahye Lee,[†] Ivan Nekrashevich,[†] Han Ju Lee,[§] Chamath Dannangoda,[∥] Karen S. Martirosyan,[∥] T. Randall Lee,[*,§] and Dmitri Litvinov[*,†,‡]

[†]Materials Science and Engineering, [‡]Electrical and Computer Engineering, [§]Department of Chemistry and the Texas Center for Superconductivity, University of Houston, 4800 Calhoun Road, Houston, Texas 77204-5003, United States

[∥]Department of Physics, University of Texas Rio Grande Valley, Brownsville, Texas 78520, United States

Supporting Information

ABSTRACT: Single or a-few-atoms-thick sheets of graphene and graphene oxide (GO) exhibit a range of unique mechanical, optical, thermal, and electrical properties. While these properties have been extensively studied, research into the magnetics of graphene and GO systems is still in its early stages. A number of theoretical studies, which have yet to be verified experimentally, predict that various types of magnetism can be induced in otherwise diamagnetic carbon systems through (1) the introduction of defects in conjugated carbon networks (e.g., vacancies and covalently bonded functional groups that are abundantly present in GO), (2) the substitution of heteroatoms, and (3) edge effects. Although pristine graphene shows in many respects some of the most interesting features, unlike GO, it is difficult to produce pristine graphene in sufficient quantities to characterize or harvest its magnetic properties for real-world applications. In this study, we examine derivatives of graphene and describe an approach to induce a defect-based frustrated magnetic (spin-glass) phase in GO powders using a rather simple chemical process of surface modification by sodium sulfate (SS). Magnetization as a function of applied field (M-H loops) and the temperature dependence of magnetization in zero and nonzero field-cooling experiments show behavior that is typical for superparamagnets and frustrated magnetic systems such as spin glasses. Characterization of the magnetic properties paired with XPS and Raman spectroscopy reveal the nature of the chemical bonds and suggest that the exposure of paramagnetic GO to SS leads to the development of magnetic sites across the GO surface that form spin-glass-like phases similar to other spin-glass phases in highly disordered magnetic materials.

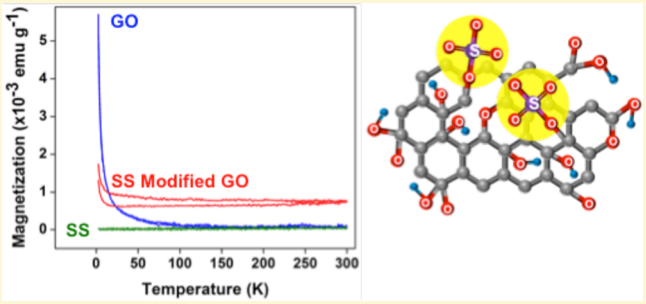

INTRODUCTION

Graphene is composed of a conjugated carbon atom network with a honeycomb crystal lattice, bond lengths of 1.42 Å, and a thickness of only one atom.[1] Certain properties of graphene, such as low spin−orbital coupling and zero nuclear spin of the naturally abundant ^{12}C isotope, are favorable for spintronic applications. These properties give rise to a large spin diffusion length and long coherence times,[2−4] which are crucial for quantum information processing and quantum computing.[2,5]

Prior research has shown that graphene possesses unique electrical,[6] mechanical,[7] thermal,[8] and optical properties,[9] but there are few studies regarding the magnetic properties of graphene. Consequently, there is a need to advance the understanding of the magnetic properties of graphene and its derivatives and to develop the ability to tune such properties, enabling prospective applications of graphene-based materials in nanomagnetoelectronic, spintronic[10−12] (such as spin memory, transistors, and perhaps solid−state qubits),[2,3,11,13] magnetoresistance, and magnetic memory devices.[13−16]

Recent research has shown that defect-free graphene exhibits no detectable magnetic behavior. Apparently, irregularities in the carbon bonding network, such as covalently bonded moieties that disrupt the network,[15] along with other defects and structural discontinuities in the aromatic network, are essential for magnetism to be present in graphene.[16] These irregularities are known to play an important role because they can induce spin polarization in systems that typically possess high levels of symmetry.[17] Therefore, developing controlled methods of disrupting the graphene carbon bonding network is essential for inducing and tuning the magnetic properties. For practical applications,[18] it is also important that the targeted magnetic states are stable at room temperature.

A more detailed analysis of the root causes for the magnetism exhibited by certain forms of graphene can be conducted by categorizing these causes into three types: defects associated with the graphene atomic structure (topological defects),[17−19] defects caused by atoms/molecules attached to graphene or substitutuent C atoms,[20−22] and irregularities at the edges[20] of

Received: November 7, 2016
Revised: March 11, 2017
Published: April 3, 2017

DOI: 10.1021/acs.chemmater.6b04748
Chem. Mater. 2017, 29, 3873−3882

the graphene sheet. Unfortunately, studies providing experimental magnetic data are rare.

Chemical functionalization[23] is one of the most experimentally accessible ways to introduce systematic defects into pristine graphene. This method is not only useful for introducing defects, but it is also efficient for dispersing graphene in organic solvents or water. In addition, it can be used to produce nanocomposites and to decorate graphene with various molecules suitable for various applications. For example, diazonium salts have been widely used for the chemical functionalization of graphene;[24] Haddon et al. demonstrated that diazonium functionalization of graphene on a "substrate" can be used to tune the magnetic properties.[25,26] Separately, other researchers have focused on "free-standing" graphene sheets, rather than graphene on a substrate;[27] however, there was no analysis of the magnetic properties in these reports. Besides diazonium salts, Chua et al. recently explored the modification of graphene with thiols,[28] but again performed no magnetic characterization of these samples. While these methods are well understood and accepted, the production of quantities of functionalized graphene sufficient for magnetic characterization and in eventual technological applications remains an ongoing challenge.

In this study, we demonstrate experimentally that nonmagnetic sodium sulfate (SS) induces a spin-glass-like magnetic phase in graphene oxide (GO) by means of a simple chemical functionalization process. A previous study showed that the modification of GO with sulfate gave rise to an improvement in the electron-transport properties;[29] this observation led us to explore the use of the sulfate group to modify GO with respect to studies of magnetism. Specifically, SS, which is nontoxic (i.e., "green"), readily available, inexpensive, and stable, was used to modify GO in this study. Oxidized graphene (or GO) flakes prepared in an aqueous phase using Hummer's method dispersed in an aqueous phase (please see the Supporting Information for details) were used in this study. Several different oxygen functional groups are present on both sides of the GO basal planes and edges, providing ample sites for chemical reaction and functionalization.[30] We used SS to modify GO, which allowed a systematic investigation of the impact of this chemical species on the magnetic properties of GO.

EXPERIMENTAL SECTION

A 15-mL portion of a degassed and homogeneously dispersed 0.24 wt % GO aqueous solution was mixed with 0.15 g of SS. This mixture was protected from the atmosphere to avoid further oxidation by purging the solution with Ar for 30 min. Separate 15-mL samples of this mixture were prepared and then either maintained at 23 °C or heated to 40 or 80 °C for 48 h in a closed system while stirring. The resulting solutions appeared light brown (23 °C), brown (40 °C), or black (80 °C), depending on the reaction conditions. After cooling to room temperature, these solutions were opened to the atmosphere for the washing steps. The GO products in aqueous solution were then centrifuged for 1 h at 10 000 rpm, with the resulting supernatant being discarded, and the GO products redispersed in acetone. The washing steps were repeated using acetone, acetonitrile, ethanol, and Milli-Q water to remove any excess SS in solution or any physisorbed SS. Samples of GO processed without adding SS were also prepared as described above and washed using the same procedure to ensure that these control samples were exposed to the same conditions as the samples that contained SS. The washed GO samples were finally redispersed in Milli-Q water followed by drying in a vacuum freeze-dryer. The final products were either a brown or black fluffy powder, depending on the degree of deoxygenation of the GO (i.e., a more deoxygenated GO sample appeared as a blackish powder). All characterization was conducted on these final powders. The sample abbreviations used in this report are shown in Table 1.

Table 1. Abbreviations for the GO Samples and Their Reaction Conditions

sample abbreviation	treated with SS	reaction temperature (°C)
GO-23	no	23
GO-40	no	40
GO-80	no	80
SS-GO-23	yes	23
SS-GO-40	yes	40
SS-GO-80	yes	80

Instrumental Methods Used to Characterize the Graphene Oxide Samples. A Quantum Design Ever Cool-II Physical Property Measurement System (PPMS) was used to collect the vibrating sample magnetometry (VSM) data, which provided the hysteresis loops, the zero-field-cooled (ZFC) curves, and the field-cooled (FC) curves. High-resolution X-ray photoelectron spectroscopy (XPS) data were collected using a Physical Electronics Model 5700 XPS instrument. Raman spectra were collected using a 532 nm laser, which was initially expanded and then focused onto the sample of an inverted microscope (Olympus IX71) through an epi-Raman 60× objective lens. The scattered Raman light from the sample was filtered using a long pass filter (Semrock) and collected by a spectrograph (Acton 300i) and CCD (Princeton 400BR). Infrared (IR) spectra were collected using a Thermo Scientific Nicolet IS5 infrared spectrometer; the spectral data were acquired using 48 scans at a resolution of 4 cm^{-1}.

RESULTS AND DISCUSSION

The samples described in Table 1, and commercially obtained samples of SS were analyzed for this study. In Table 1, the number following the GO notation corresponds to the temperature in degrees Celsius, at which the samples were treated both with and without SS as described in the Experimental Section. The O−S bond from RO−SO_3^- can be cleaved at temperatures ranging from 70 to 100 °C, depending on the nature of the alkyl substituent. Therefore, three different temperatures were tested: 23 °C to represent ambient temperature, 40 °C as a temperature below which the O−S bond undergoes cleavage, and 80 °C as a temperature above which the O−S bond undergoes cleavage.

As observed for SS-GO-40 in Figure 1, the opening at positive magnetic field of the M−H loops is typical in ferro/ferrimagnetic and spin-glass systems due to the exchange interaction (direct or indirect such as RKKY) present in the system.[31]

Characterization of Magnetic Properties. We obtained the magnetization (M−H) loops at room temperature shown in Figure 1A for the samples listed in Table 1. The linear part of the signal was subtracted as described elsewhere,[22,26,32] and the resulting hysteresis loops are shown in Figure 1B to illustrate the saturation magnetization. As can be determined from the loops, unmodified GO samples show little or no hysteretic behavior, which is typical for paramagnets. The pure SS compound measured alone has a negligible magnetic moment (see Figure 1B). The saturation magnetization values (M_S) and susceptibility (χ) for all of the samples were obtained from Figure 1B, and the resulting data were plotted in Figure 2. Samples modified with SS showed higher M_S and χ (at $H = 0$) values compared to non-SS-modified GO samples at room temperature. Compared to GO-23, the M_S values increased 3,

DOI: 10.1021/acs.chemmater.6b04748
Chem. Mater. 2017, 29, 3873−3882

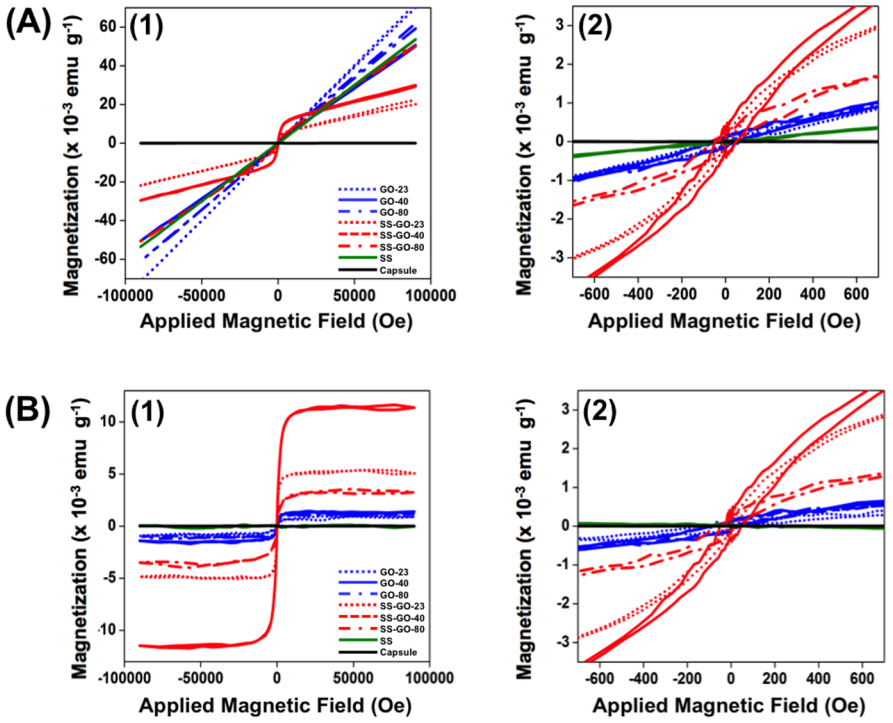

Figure 1. Hysteresis loops from applied magnetic fields of −9 T to +9 T collected at 300 K for the six samples provided in Table 1, for sodium sulfate, and for the capsule used in these experiments: (A) after subtracting the capsule including background and (B) after subtracting the linear signal. Enlarged plots providing data for ±700 Oe from each part 1 are plotted in each part 2.

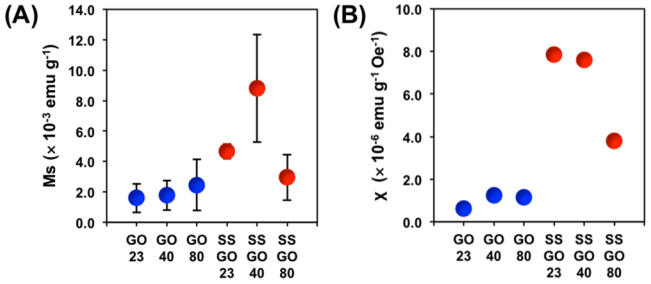

Figure 2. Magnetic data from Figure 1B: data collected from two samples generated under each set of reaction conditions, with two independent measurements for each sample. (A) Saturation magnetization, M_S (emu g^{-1}), and (B) magnetic susceptibility, χ (emu g^{-1} Oe^{-1}), which is the slope of the M−H curves (Figure 1B) at zero applied external magnetic field. Error bars are not visible when the error falls within the symbols.

6, and 2 times, and the χ values increased 13, 12, and 6 times for SS-GO-23, SS-GO-40, and SS-GO-80, respectively, upon modification with SS. One possible reason for the nonlinear behavior of the magnetic moment with respect to the reaction temperature is the presence of two concurring processes during the functionalization reaction: (1) Binding of the SS groups to the GO basal plane potentially increases the number of localized spin states, and the O−S bond of RO−SO_3^- can be cleaved at temperatures ranging from 70 to 100 °C. (2) The hydrothermal reduction of GO causes a decrease in the number of reaction sites. The values of susceptibility obtained in our experiments are within a reasonable range when compared to values reported previously.[33−35] The difference between the loops of SS-modified and untreated GO flakes indicates the emergence of a magnetic phase that is absent in both GO and SS measured separately.

These results agree with previous studies where both the introduction of chemical agents and thermal annealing play considerable roles in tuning the magnetic properties.[30,36] Further, the magnitude of magnetic moment alone is not an exhaustive measure of the magnetic properties of the system. To distinguish/isolate the different magnetic phases present in the materials and elucidate the nature (vacancies and impurities) of the magnetic interactions in the system, additional measurements are necessary. To gain better insight into the magnetic properties of both GO and SS-modified-GO, we performed a set of additional magnetic measurements that allowed us to collect zero-field-cooled (ZFC) and field-cooled (FC) curves (magnetization as a function of temperature), which are shown in Figure 3. The ZFC−FC curves provide a method for measuring the magnetization while the temperature is rising or decreasing in the presence of an external magnetic field. The analysis of these data does not require the subtraction of the linear signal, which renders these results relatively free from artifacts.[37]

Analysis of the dependence of the magnetic moment of functionalized and unmodified GO samples on temperature allows identification of the magnetic phases present in the samples. The behavior of the unmodified GO samples is consistent with a paramagnetic material[38] and can be fitted with a modified form of Curie's law, which is described by eq 1:

$$M = \frac{C}{T - \theta} + \chi_0 \quad (1)$$

where M is the magnetic moment, T is the absolute temperature, θ is the Curie−Weiss temperature, C is a material-dependent constant, and χ_0 is a temperature-independent term. The linear dependence of magnetization on inverse temperature confirms our assumption of paramagnetism in the pristine GO samples, GO-23, GO-40, and

DOI: 10.1021/acs.chemmater.6b04748
Chem. Mater. 2017, 29, 3873−3882

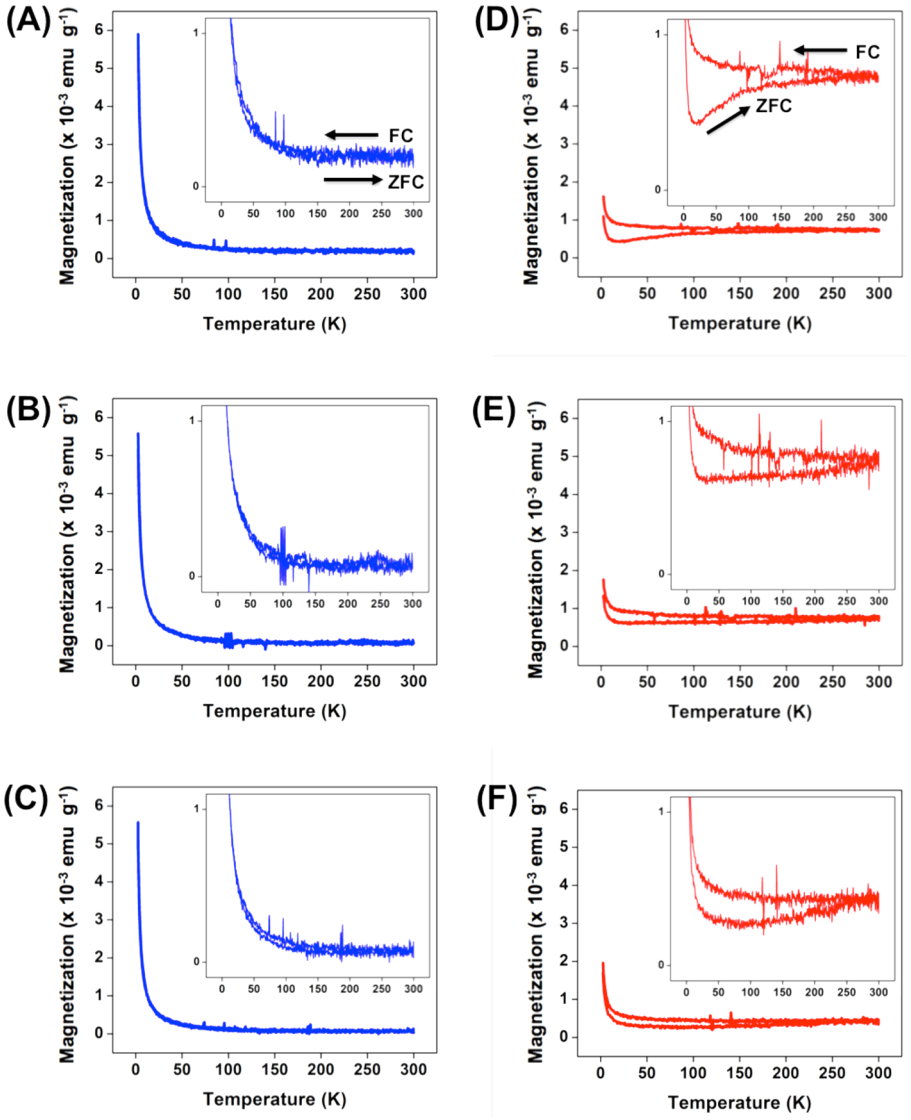

Figure 3. Zero-field-cooled (ZFC) and field-cooled (FC) data collected for all six samples described in Table 1 while applying a magnetic field of 100 Oe: (A) GO-23, (B) GO-40, (C) GO-80, (D) SS-GO-23, (E) SS-GO-40, and (F) SS-GO-80. The displayed data include background subtraction for the capsule. The insets for each plot provide an enlarged section of the data from a magnetization of 0 to 1.

Table 2. Least-Squares Fit Parameters and Corresponding Standard Deviation Values for Unmodified GO Samples

sample	C (emu*K/g)	Θ (K)	χ_0 (emu/g)	σ (C)	σ (Θ)	σ (χ_0)
GO-23	1.41×10^{-2}	0.0565	12×10^{-5}	6.7×10^{-5}	1.6×10^{-2}	1.3×10^{-6}
GO-40	1.45×10^{-2}	0.165	-2.8×10^{-6}	8.3×10^{-5}	2.1×10^{-2}	1.5×10^{-6}
GO-80	1.22×10^{-2}	0.153	1.01×10^{-5}	5.7×10^{-5}	1.5×10^{-2}	1.1×10^{-6}

GO-80 (see Figure S1 in the Supporting Information). Good agreement of the GO magnetization with eq 1 was achieved with our samples (see Table 2).

A sample of the unmodified GO used for the experiments reported herein was analyzed by ICP-MS to determine the elemental composition (see Figures S2–S5 in the Supporting Information). The average concentrations of magnetic impurities in this sample between two runs were detected as 18.9, 2.9, 0.1, and 1800.0 ppm for Fe, Ni, Co, and Mn, respectively, after subtracting the blank. Notably, the Mn arises from $KMnO_4$ used in the GO synthesis process (Hummer's method). We then took the highest values of the concentration of each element between two runs, 22.4, 3.1, 0.1, and 1800.0 ppm for Fe, Ni, Co, and Mn, respectively. On the basis of the reported values of the atomic magnetic moments of Fe (2.2 μ_B), Ni (0.6 μ_B), Co (1.7 μ_B), and Mn (1 μ_B),[31] the contribution to the total magnetic moment of the GO sample from the first three elements (2.3×10^{-2} emu/g, 8.5×10^{-4} emu/g, 7.9×10^{-5} emu/g for Fe, Ni, Co respectively) is one order of magnitude lower than the contribution from Mn (8.4×10^{-1} emu/g). Calculation of the magnetic moment arising from the paramagnetic impurities assumed that the magnetic moment of ^{12}C atoms is negligible. For example, the magnetic moment produced by Mn atoms at a concentration of 1800.0 atoms of Mn per one million atoms of ^{12}C, as measured by ICP-MS, is (1800.0 ppm Mn $\times$ 1 $\mu_B \times 0.93 \times 10^{-20}$ emu/μ_B)/

DOI: 10.1021/acs.chemmater.6b04748
Chem. Mater. 2017, 29, 3873−3882

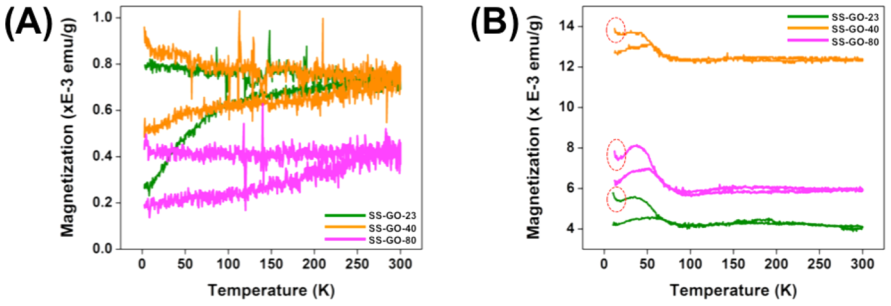

Figure 4. ZFC-FC curves of the sulfate-modified-GO samples (SS-GO-23, SS-GO-40, and SS-GO-80) with applied magnetic fields of 100 Oe (A) and 1 T (B) after subtracting the paramagnetic contributions. Regions marked with dashed lines show bends that are likely due to the deviation of magnetization of the paramagnetic phase from simple Curie's law at low temperatures and high applied fields.

(1.99264×10^{-17} g carbon) $\approx 8.4 \times 10^{-1}$ emu/g. On the basis of these calculations and the paramagnetic behavior shown in Figure 3A–C, we can conclude that most of the paramagnetic contribution in GO likely comes from Mn impurities. *Importantly, in our analyses below of SS-modified GO, we subtract the paramagnetic component of the signal arising from the metallic impurities from the total magnetic signal of SS-modified GO.*

For the SS-modified GO samples, we assume that most of the material is carbon. Therefore, 1 g of carbon contains approximately 0.5018×10^{23} atoms of carbon, and 1 emu converts to 1.0783×10^{20} μ_B. Therefore, 1 emu/g translates to 2.1488×10^{-3} μ_B/C (Bohr magnetons per carbon atom). Measured values of M_S, as shown in Figure 2, range from about 2×10^{-3} emu/g to 8×10^{-3} emu/g at 23 °C, which give magnetic moments of about 4.3×10^{-6} μ_B/C to 1.7×10^{-5} μ_B/C for the samples shown in Figure 2A. Importantly, these values are several orders of magnitude lower than the magnetic moments of rare earth elements, as discussed above. Also, this observation suggests that we are dealing with dilute magnetic systems.

There are several salient differences between the untreated samples (plots A, B, and C in Figure 3) versus the SS-treated GO samples (plots D, E, and F in Figure 3). Nonzero magnetization of the SS-treated samples can be observed at room temperature in contrast to the untreated samples, which show negligible magnetization at room temperature. Another important difference is the separation between the ZFC and FC curves. Both the ZFC and FC data follow similar trends for the untreated samples, but there is clearly a gap between the FC and ZFC curves for the SS-treated samples. The divergence between the FC and ZFC curves indicates the presence of disordered magnetism in the modified GO samples,[21] which is characteristic for magnetically frustrated systems. Therefore, the divergence that appeared only for the SS-modified GO samples suggests that the reaction with sulfate triggers a form of disordered magnetism in the sulfate-modified GO samples. Several researchers have concluded that coexisting phases are induced by disordered magnetism in modified graphene.[22,25,26,36] On the basis of our results, we propose that modification by SS introduces a spin-glass-like phase in GO.

We collected ZFC-FC curves using applied fields of 100 Oe and 1 T for the SS-modified samples, and then subtracted the paramagnetic part of the signal from the initial ZFC-FC curves to assess the properties of the spin-glass phase in greater detail (see Figure 4). Parameters of the subtracted paramagnetic component were determined from the untreated GO samples (see Figures 3A–C and Table 2). When comparing Figures 1 and 4B, please note that the background signal was not subtracted from the ZFC-FC curves, and some shifts due to the presence of background moment are possible, which can cause the slightly different magnetic moment values observed in Figure 1 and Figure 4 for the SS-GO-23 and SS-GO-80 samples at 1 T that are somewhat close in magnitude. The main purpose of Figure 4 is to illustrate the presence and change of the magnitude of the gap and shift of the transition temperature (opening of the gap) when comparing the ZFC-FC measurements made at 100 Oe and 1 T bias fields. Comparing the ZFC-FC curves obtained for each applied field, a larger gap between ZFC and FC and a shift of the point at which the curves split toward lower temperature values was observed in the case of 1 T. Such behavior is typical for frustrated magnetic systems, which further corroborates our proposal of the presence of a spin-glass phase in our samples.[39] A bend (marked with dashed lines) in the ZFC-FC curves obtained at 1 T and lower temperatures can be observed (Figure 3B, marked regions). This bend likely arises from a deviation in the paramagnetic phase behavior from simple Curie's law at high applied field and low temperature. This assumption is supported by the absence of such a jump in magnetization in the ZFC-FC curves obtained at 100 Oe, where the applied magnetic field is insufficient to saturate the paramagnetic phase. Cartoons illustrating the spins of the samples during the ZFC/FC experiments at both 100 Oe and 1 T are shown in Figures S6, S7, and S8 in the Supporting Information.

Assuming a simple general expression for the coercive field, $H_c \sim K/M$, where K is the magnetic anisotropy of a material and M is the magnetic moment, Figure 5 shows that in the low temperature range (3 to ~15 K), the behavior of the system is

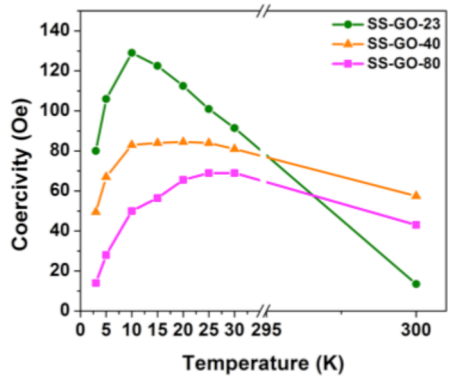

Figure 5. Coercivity values for the sulfate-modified-GO samples: SS-GO-23, SS-GO-40, and SS-GO-80. The data points were collected from the hysteresis loops in Figure 1 as an average of the *x*-intercepts.

DOI: 10.1021/acs.chemmater.6b04748
Chem. Mater. 2017, 29, 3873–3882

dominated by the rapidly decreasing ($M \sim 1/T$) magnetic moment of the near-saturated paramagnetic phase, which leads to the observed increase in coercivity. In the temperature range of ~15 to 30 K, the frustrated magnetic phase shows the strongest influence on the magnetic behavior of the system, as the moment of the paramagnetic part reaches low values leading to high values of H_c. At room temperature or above T_c (the glass transition temperature), the system again shows more paramagnetic character as the spin-glass is "softened" by thermal agitation.

The presence of the frustrated magnetic structure in SS-modified GO is possibly due to the formation of localized electron states at the sites induced by the covalently bound electron-withdrawing sodium sulfate groups. A relatively low ratio of sulfur to carbon (~0.01 to 0.06 depending on the reaction temperature; vide infra) suggests the case of a dilute magnetic system with interaction between sodium sulfate-induced magnetic sites governed by Ruderman−Kittel−Kasuya−Yosida (RKKY) interactions.[40,41] The S/C ratios noted above are consistent with an average distance between sodium sulfate groups of about 2.5 and 6 graphene lattice constants, respectively. Dependence of the strength of the RKKY interaction on the distance between magnetic impurities and the oscillatory behavior of its sign (positive or negative) leads to the spin-glass behavior of the system. The presence of a ferromagnetic/antiferromagnetic phase requires the existence of well-defined long-range order of the defects in the system, which is unlikely considering the stochastic nature of how the magnetic defects are formed. For ferro/ferri/antiferromagnetism to exist in the system, localized uncompensated spins should form a regular structure as in normal crystals with well-defined translational symmetry, which is improbable for our samples. In our GO and SS-GO samples, magnetic defects are randomly distributed, and some neighboring localized spins are coupled ferromagnetically while others are coupled antiferromagnetically due to the fact that the RKKY interaction depends on the distance between magnetic impurities; furthermore, the strength of this coupling depends on distance due to the nature of RKKY. These features make the presence of pure ferromagnetic or antiferromagnetic phases in our samples virtually impossible, and a spin-glass is the most likely candidate to rationalize the observed magnetic properties.

To gain a better understanding of the trends associated with the magnetic properties, we further analyzed the samples by X-ray photoelectron spectroscopy (XPS), Raman spectroscopy, and infrared (IR) spectroscopy.

Structural Characterization Using XPS. The C 1s, O 1s, and S 2p spectra obtained from the samples were collected (see Figures S9 and S10 and Table S1 in the Supporting Information). On the basis of these spectra, we plotted the intensities of the C 1s peaks in Figure S11. In particular, Figures S11c and S11d in the Supporting Information facilitate a comparison of the trends (see pages S16 and S17) in the oxidized carbons (e.g., epoxy-based and hydroxyl-based) versus the unoxidized sp^2 framework carbons. Separately, Figure S12 in the Supporting Information shows a layered plot of the sulfur spectra to facilitate comparison of the sulfur content and species in all of the samples. The relative counts for the oxidized carbons when compared to the framework carbons (sp^2) of GO decreased as the reaction temperature increased from 23 to 40 and then to 80 °C. For SS-GO-23, SS-GO-40, and SS-GO-80, compared to GO-23, the plots in Figure S11 show that the O/C ratio decreased by 0%, 4%, and 7% for 23 °C, 40 °C, and 80 °C, respectively; furthermore, the plots in Figure S12 show that the S/C ratio increased 3 times, 18 times, and 8 times, respectively.

Structural Characterization Using Raman Spectroscopy. Characterization of graphene by Raman spectroscopy reveals various structural details, such as crystalline order[42,43] and average crystal size.[44−46] Moreover, this technique is nondestructive with rapid data collection. Raman spectroscopy has also been used to monitor doping, defects, strain, and the chemical functionalization of graphene.[47−49] There is a unique resonance Raman effect arising from coupling of the excitation source with a particular interband transition in graphene. However, in the case of ideal defect-free graphene, there is no resonance effect, and the peak intensity ratio (I_D/I_G) in the Raman spectrum provides a simple tool with which to interpret the relative disorder of the structure.[49]

The two most significant bands in the Raman spectra of graphitic materials are identified as the D and G bands, and these characteristic bands can reveal how the different reaction temperatures, and the addition of SS, affect GO structurally. The G band (E_{2g}), a doubly degenerate phonon mode at the Brillouin zone center, originates from in-plain vibrations of the sp^2 carbons and is generally observed at ~1575 cm^{-1}.[50] The D band (A_{1g}) is also in-plain and is active and typically observed at ~1350 cm^{-1}. In the Raman spectra of graphene and its derivatives, the ratio of I_D/I_G provides useful information regarding whether the framework of graphene has been modified by the attachment or detachment of molecules. It has been shown that the increase in I_D/I_G is due either to deoxygenation of GO or to the presence of covalently attached materials to GO.[30] The observation of a strong D band in graphene-based samples suggests that the structure has a large number of defects and disorder.[19] In this study, we observed an increase in the I_D/I_G ratio when the GO was treated at high temperatures in aqueous solution and an even greater increase when the GO was treated at high temperatures in the presence of SS as shown in Figure 6.

The I_D/I_G ratio increased in the order of GO-23, GO-40, and GO-80, a result consistent with the XPS data from the hydrothermal deoxygenation (see Figure S11a in the Supporting Information). As expected, the oxidized carbon ratio decreased with an increase in the reaction temperature, which is consistent with the observed I_D/I_G ratio obtained by Raman spectroscopy. Furthermore, the GO samples that were exposed to SS (SS-GO-23, SS-GO-40, and SS-GO-80) have more defects than the GO samples that were not exposed to SS under the same thermal conditions due to the sulfate moieties covalently bonding to GO.[29] The I_D/I_G data indicate further that the SS-GO-80 samples have more defects than the other samples, even though the number of sulfate groups attached is less than that for the SS-GO-40 samples, because the SS moiety has a greater likelihood of being detached at temperatures above 40 °C.[51] In other words, while more SS moieties can become attached at 80 °C, the reverse reaction is also facile at that temperature, leaving more defects on SS-GO-80; this model is supported by the results shown in Table S2 in the Supporting Information. In short, the SS-GO-80 samples have more defects than the other samples but also have fewer attached sulfate moieties. This model is also consistent with the observation that the SS-GO-80 samples have the lowest M_S (see Figure 2); notably, the magnetization arises from a combination of attached sulfate species and the presence of various types of defects (e.g., defects caused by the process of

DOI: 10.1021/acs.chemmater.6b04748
Chem. Mater. 2017, 29, 3873−3882

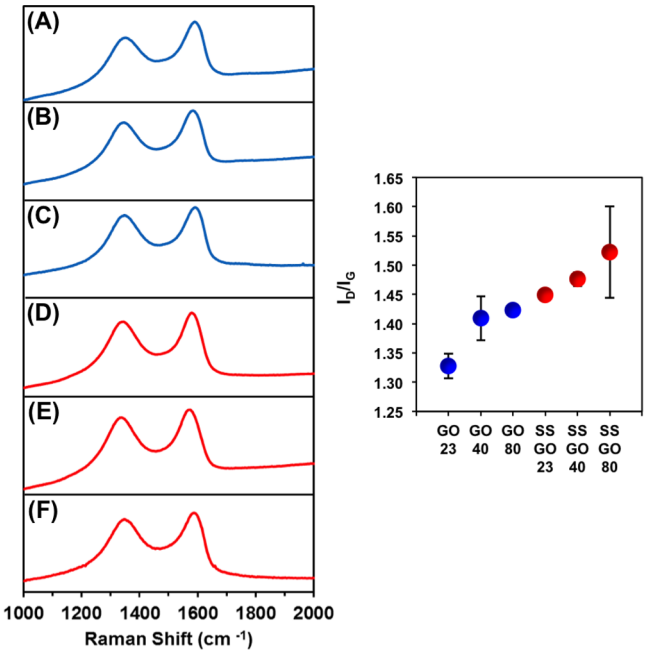

Figure 6. Raman spectra (left) and I_D/I_G data (right) obtained from the Raman spectra of graphene oxide samples prepared under various reaction conditions. (A) GO-23, (B) GO-40, (C) GO-80, (D) SS-GO-23, (E) SS-GO-40, and (F) SS-GO-80. The error bars represent the standard deviation for data collected from three independent samples; invisible error bars fall within the symbols.

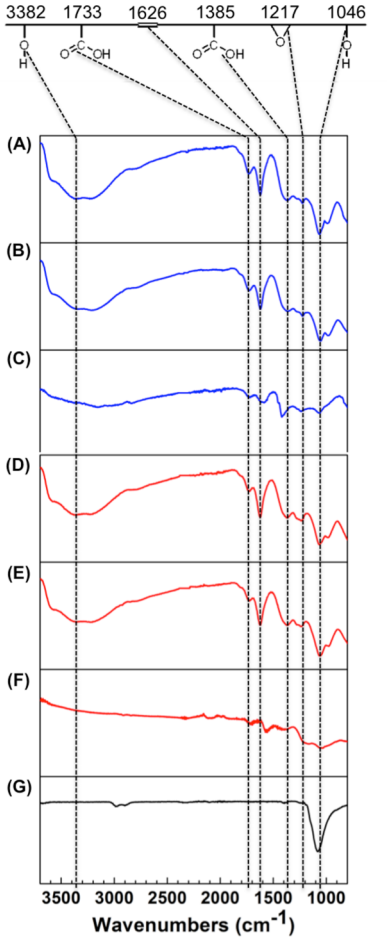

Figure 7. IR spectra of graphene oxide samples prepared under various reaction conditions along with a spectrum of sodium sulfate: (A) GO-23, (B) GO-40, (C) GO-80, (D) SS-GO-23, (E) SS-GO-40, (F) SS-GO-80, and (G) SS.

sulfate attachment/detachment and hydrothermal deoxygenation). In summary, the deoxygenation of GO and sulfate grafting to GO leads to an enhanced number of sp^2 carbon domains, but with smaller sizes, which increases the I_D/I_G ratio.[29]

Functional Group Characterization Using Infrared Spectroscopy. The six peaks shown in Figure 7 associated with readily identified structural features for these samples are centered at ~3400, 1730, 1620, 1385, 1217, and 1045 cm^{-1}, which can be assigned to the hydroxyl O−H bond, the C═O bond from COOH, the aromatic C═C bonds from skeletal vibrations of sections of the sp^2 framework of GO, the C−OH bond from COOH, the C−O bond from epoxy rings, and the C−O bond from hydroxyl stretching vibrations, respectively.[21,52−54] For the SS spectrum, the most significant peak located at 1083 cm^{-1} arises from the S═O bond of sulfate.

There are a few significant changes between the GO samples treated with SS compared to the samples not treated with SS. The most significant observation is that the samples exposed to heating are more deoxygenated with increasing reaction temperature (especially 80 °C), which is consistent with the XPS and Raman data. This effect can be attributed to hydrothermal deoxygenation.[21] The O−H stretching associated with the hydroxyl group (~3400 cm^{-1}) shows the greatest reductions (see, for example, the spectra for the GO-80 and SS-GO-80 samples in Figure 7C and F, respectively). Also, the peaks attributed to the C−O (1385 cm^{-1}) and C═O (~1730 cm^{-1}) bonds from COOH are significantly diminished for the samples treated at 80 °C. The peak for the C−O bond for the carboxylic acid groups, which is located at ~1370 cm^{-1} for GO-23, exhibits a blue shift to ~1410 cm^{-1} for the GO-80 and SS-GO-80 samples, perhaps due to the reduction in nearby hydroxyl groups as described above.[52] The peak at ~1580 cm^{-1} can be assigned to the sp^2-hybridized C═C backbone in GO, while the peak at ~1600 cm^{-1} arises from an oxidized graphene framework.[55,56] Therefore, the IR spectra of the samples treated at 80 °C, GO-80 and SS-GO-80, exhibit a red shift from ~1626 to ~1585 cm^{-1} upon heating above 40 °C.[55,56]

With regard to an analysis of the sulfate-based peaks in the SS-modified samples, the spectra show no obvious peak at 1083 cm^{-1} nor any additional peaks at 950−1300 cm^{-1}, which are characteristic of organic sulfates (for which the S−O ν_{as} band appears at 1200 and 1300 cm^{-1}, and the S−O ν_s band appears at 950 and 1100 cm^{-1}).[57] Our inability to observe these peaks can be attributed to (1) the low concentration of sulfate species in the samples and (2) overlapping peak intensities over this range of frequencies due to functional group contributions from various C−O stretching modes (e.g., hydroxyl and epoxy/ether).

Acid/Base Stability/Dipersibility Test. We performed stability/dispersibility tests to verify that the sulfate groups were covalently attached to the GO. Prior reports have noted that GO is dispersible in an aqueous phase due to the presence of carboxylic acid groups that readily ionize to form carboxylate (COO^-) groups.[58] The GO sheets can be stably dispersed above a pH value of ~4, with some variance in the exact pH value depending on the chemical environment near the carboxylic acid moieties (e.g., functional groups that are present

DOI: 10.1021/acs.chemmater.6b04748
Chem. Mater. 2017, 29, 3873−3882

and the proximity of these functional groups to each other).[59] Another important consideration is that these moieties typically populate the edges of GO.[58] Therefore, GO samples tend to aggregate and then precipitate in aqueous solution as the pH drops below a value of ~4 since the $-COO^-$ anions are protonated and become −COOH, enabling the formation of hydrogen bonds between GO flakes. However, the sulfate-functionalized GO are less likely to aggregate under these conditions because the surface-bound sulfate group has a lower pK_a value than the graphene-bound carboxylate group.[39] Therefore, we anticipated that the sulfate-functionalized GO samples would exhibit enhanced stability under acidic conditions. With this knowledge to support our efforts, we conducted tests on all of the GO samples at varying pH conditions. Selected pH solutions were prepared with NaOH and HCl at concentrations ranging from 2×10^{-6} M to 2×10^{-1} M, and then 1 mL of each of these solutions was mixed with 1 mL of each of the six samples. Figure 8 shows the data

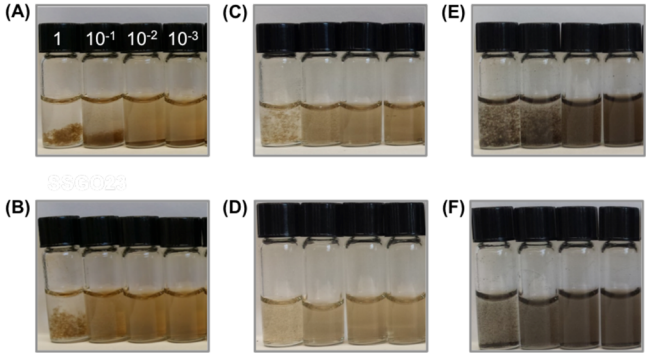

Figure 8. Photographs of a series of solutions of all six samples described in Table 1 over the range of 10^{-3} M to 1 M aqueous HCl solutions: (A) GO-23, (B) SS-GO-23, (C) GO-40, (D) SS-GO-40, (E) GO-80, and (F) SS-GO-80.

obtained over the range of 10^{-3} M to 1 M for the HCl solutions; the results from the entire pH stability test from 10^{-1} M NaOH to 1 M HCl are illustrated in Figure S14 of the Supporting Information.

As shown in Figures 8A, 8C, and 8E, the GO samples untreated with SS (GO-23, GO-40, and GO-80) started to aggregate and then precipitate in each of the solutions prepared by adding 1 mL of 2×10^{-2} or 2×10^{-1} M HCl to the GO solution. In contrast, the sulfate-functionalized GO samples (SS-GO-23, SS-GO-40, and SS-GO-80) were still well dispersed in solution at the lower pH values, including the samples that had been exposed to elevated temperatures. However, for the most acidic conditions, those samples also started to aggregate, as shown in Figures 8B, 8D, and 8F.

CONCLUSIONS

This report described a novel, simple, and accessible technique for the functionalization of graphene oxide by means of moderate thermal treatment with sodium sulfate. There are many factors that can plausibly affect the magnetic properties of GO, including edges, defects, and oxygen functional groups naturally present in the system. While we observed a relatively moderate increase of the saturation magnetization of SS-modified GO compared to untreated-GO samples, important *qualitative* differences should be noted. A comparison of the ZFC−FC curves for untreated GO (no gap) and SS-modified GO samples reveals the opening of the gap, which depends of the bias field. This observation allows us to conclude that functionalization with SS causes an important change in the type of magnetic phase in these derivatives of graphene. Also, since we used the same GO precursor for SS modification, we can single out SS as the main component that gives rise to the change of the magnetic phase. The results suggest that such modification altered the electronic structure of GO and led to the formation of a frustrated magnetic phase, where magnetic defects and localized spins are coupled through an RKKY interaction. From the results, we can conclude that SS functionalization played a critical role in enabling the long-range RKKY coupling between the magnetic impurities in graphene oxide. The emergence of a frustrated magnetic phase was supported by a systematic increase in the saturation magnetization and finite coercivity observed at room temperature. The random distribution of structural defects naturally abundant in GO, localized electronic states, and oscillatory nature of the long-range RKKY interaction allowed us to propose that the observed magnetic phase exhibited a spin-glass nature. Our proposal was further supported by the observation of irreversibility in the ZFC−FC curves obtained at 100 Oe and 1 T. According to the results in this paper along with recent reports from other researchers, we conclude that structural defects, bound oxygen, and sulfate-functionalization enabled a unique and interesting modification of the magnetic properties of graphene oxide. Our research paves the way for further exploration of the capacity of electron-withdrawing/donating groups and structural defects in conjugated carbon nanosystems for tuning their magnetic and electronic properties.

ASSOCIATED CONTENT

Supporting Information

The Supporting Information is available free of charge on the ACS Publications website at DOI: 10.1021/acs.chemmater.6b04748.

Detailed descriptions of the materials and analysis procedures and results for this research (PDF)

AUTHOR INFORMATION

Corresponding Authors

*E-mail: trlee@uh.edu.
*E-mail: litvinov@uh.edu.

ORCID

T. Randall Lee: 0000-0001-9584-8861

Notes

The authors declare no competing financial interest.

ACKNOWLEDGMENTS

We thank the Robert A. Welch Foundation (grant no. E-1320) and the Texas Center for Superconductivity at the University of Houston, the Cancer Prevention Research Institute of Texas (Grant No. RP150343), and the National Science Foundation (Grant CBET-0932971) for generous support. We also thank Prof. Wei-Chuan Shih and Ms. Jingting Li for assistance with the collection of the Raman spectra.

REFERENCES

(1) Tuinstra, F.; Koenig, J. L. Raman Spectrum of Graphite. *J. Chem. Phys.* **1970**, *53*, 1126−1130.
(2) Wang, W. L.; Meng, S.; Kaxiras, E. Graphene NanoFlakes with Large Spin. *Nano Lett.* **2008**, *8*, 241−245.

DOI: 10.1021/acs.chemmater.6b04748
Chem. Mater. 2017, 29, 3873−3882

(3) Yazyev, O. V. Hyperfine Interactions in Graphene and Related Carbon Nanostructures. *Nano Lett.* **2008**, *8*, 1011−1015.
(4) Fischer, J.; Trauzettel, B.; Loss, D. Hyperfine Interaction and Electron-spin Decoherence in Graphene and Carbon Nanotube Quantum Dots. *Phys. Rev. B: Condens. Matter Mater. Phys.* **2009**, *80*, 155401.
(5) Trauzettel, B.; Bulaev, D. V.; Loss, D.; Burkard, G. Spin Qubits in Graphene Quantum Dots. *Nat. Phys.* **2007**, *3*, 192−196.
(6) Niyogi, S.; Bekyarova, E.; Itkis, M. E.; Zhang, H.; Shepperd, K.; Hicks, J.; Sprinkle, M.; Berger, C.; Lau, C. N.; deHeer, W. A.; Conrad, E. H.; Haddon, R. C. Spectroscopy of Covalently Functionalized Graphene. *Nano Lett.* **2010**, *10*, 4061−4066.
(7) Gomez-Navarro, C.; Burghard, M.; Kern, K. Elastic Properties of Chemically Derived Single Graphene Sheets. *Nano Lett.* **2008**, *8*, 2045−2049.
(8) Balandin, A. A. Thermal Properties of Graphene and Nanostructured Carbon Materials. *Nat. Mater.* **2011**, *10*, 569−581.
(9) Bonaccorso, F.; Sun, Z.; Hasan, T.; Ferrari, A. C. Graphene Photonics and Optoelectronics. *Nat. Photonics* **2010**, *4*, 611−622.
(10) Wolf, S. A.; Awschalom, D. D.; Buhrman, R. A.; Daughton, J. M.; von Molnar, S.; Roukes, M. L.; Chtchelkanova, A. Y.; Treger, D. M. Spintronics: a Spin-based Electronics Vision for the Future. *Science* **2001**, *294*, 1488−1495.
(11) Awschalom, D. D.; Flatté, M. E. Challenges for Semiconductor Spintronics. *Nat. Phys.* **2007**, *3*, 153−159.
(12) Chappert, C.; Fert, A.; Van Dau, F. N. The Emergence of Spin Electronics in Data Storage. *Nat. Mater.* **2007**, *6*, 813−823.
(13) Wang, Z.; Eigler, S.; Ishii, Y.; Hu, Y.; Papp, C.; Lytken, O.; Steinrück, H.-P.; Halik, M. A. Facile Approach to Synthesize an Oxo-Functionalized Graphene/Polymer Composite for Low-Voltage Operating Memory Devices. *J. Mater. Chem. C* **2015**, *3*, 8595−8604.
(14) Hong, A. J.; Song, E. B.; Yu, H. S.; Allen, M. J.; Kim, J.; Fowler, J. D.; Wassei, J. K.; Park, Y.; Wang, Y.; Zou, J.; Kaner, R. B.; Weiller, B. H.; Wang, K. L. Graphene Flash Memory. *ACS Nano* **2011**, *5*, 7812−7817.
(15) Li, W.; Zhao, M.; Xia, Y.; Zhang, R.; Mu, Y. Covalent-Adsorption Induced Magnetism in Graphene. *J. Mater. Chem.* **2009**, *19*, 9274−9282.
(16) Alexandre, S. S.; Lucio, A. D.; Neto, A. H. C.; Nunes, R. W. Correlated Magnetic States in Extended One-Dimensional Defects in Graphene. *Nano Lett.* **2012**, *12*, 5097−5102.
(17) Yazyev, O. V.; Helm, L. Defect-Induced Magnetism in Graphene. *Phys. Rev. B: Condens. Matter Mater. Phys.* **2007**, *75*, 125408.
(18) Wang, W. L.; Yazyev, O. V.; Meng, S.; Kaxiras, E. Topological Frustration in Graphene Nanoflakes: Magnetic Order and Spin Logic Devices. *Phys. Rev. Lett.* **2009**, *102*, 157201.
(19) López-Sancho, M. P.; de Juan, F.; Vozmediano, M. A. H. Magnetic Moments in the Presence of Topological Defects in Graphene. *Phys. Rev. B: Condens. Matter Mater. Phys.* **2009**, *79*, 075413.
(20) Boukhvalov, D. W.; Katsnelson, M. I. Chemical Functionalization of Graphene with Defects. *Nano Lett.* **2008**, *8*, 4373−4379.
(21) Sarkar, S. K.; Raul, K. K.; Pradhan, S. S.; Basu, S.; Nayak, A. Magnetic Properties of Graphite Oxide and Reduced Graphene Oxide. *Phys. E* **2014**, *64*, 78−82.
(22) Sun, P.; Wang, K.; Wei, J.; Zhong, M.; Wu, D.; Zhu, H. Magnetic Transitions in Graphene Derivatives. *Nano Res.* **2014**, *7*, 1507−1518.
(23) Chua, C.; Pumera, M. Covalent Chemistry on Graphene. *Chem. Soc. Rev.* **2013**, *42*, 3222−3233.
(24) Bekyarova, E.; Itkis, M. E.; Ramesh, P.; Berger, C.; Sprinkle, M.; De Heer, W. A.; Haddon, R. C. Chemical Modification of Epitaxial Graphene: Spontaneous Grafting of Aryl Groups. *J. Am. Chem. Soc.* **2009**, *131*, 1336−1337.
(25) Hong, J.; Niyogi, S.; Bekyarova, E.; Itkis, M. E.; Ramesh, P.; Amos, N.; Litvinov, D.; Berger, C.; de Heer, W. A.; Khizroev, S.; Haddon, R. C. Effect of Nitrophenyl Functionalization on the Magnetic Properties of Epitaxial Graphene. *Small* **2011**, *7*, 1175−1180.
(26) Hong, J.; Bekyarova, E.; de Heer, W. A.; Haddon, R. C.; Khizroev, S. Chemically Engineered Graphene-Based 2D Organic Molecular Magnet. *ACS Nano* **2013**, *7*, 10011−10022.
(27) Englert, J. M.; Dotzer, C.; Yang, G.; Schmid, M.; Papp, C.; Gottfried, J. M.; Steinrück, H.-P.; Spiecker, E.; Hauke, F.; Hirsch, A. Covalent Bulk Functionalization of Graphene. *Nat. Chem.* **2011**, *3*, 279−286.
(28) Chua, C. K.; Pumera, M. Monothiolation and Reduction of Graphene Oxide via One-Pot Synthesis: Hybrid Catalyst for Oxygen Reduction. *ACS Nano* **2015**, *9*, 4193−4199.
(29) Liu, J.; Xue, Y.; Dai, L. Sulfated Graphene Oxide as a Hole-Extraction Layer in High Performance Polymer Solar Cells. *J. Phys. Chem. Lett.* **2012**, *3*, 1928−1933.
(30) Khurana, G.; Kumar, N.; Kotnala, R. K.; Nautiyal, T.; Katiyar, R. S. Temperature Tuned Defect Induced Magnetism in Reduced Graphene Oxide. *Nanoscale* **2013**, *5*, 3346−3351.
(31) Bozorth, M. R. *Ferromagnetism*; IEEE Press: Piscataway, NJ, 1993.
(32) Liang, J.; Xu, Y.; Sui, D.; Zhang, L.; Huang, Y.; Ma, Y.; Li, F.; Chen, Y. Flexible, Magnetic, and Electrically Conductive Graphene/Fe_3O_4 Paper and Its Application for Magnetic-Controlled Switched. *J. Phys. Chem. C* **2010**, *114*, 17465−17471.
(33) Liu, Y.; Tang, N.; Wan, X.; Feng, Q.; Li, M.; Xu, Q.; Liu, F.; Du, Y. Realization of Ferromagnetic Graphene Oxide with High Magnetization by Doping Graphene Oxide with Nitrogen. *Sci. Rep.* **2013**, *3*, 2566.
(34) Govind Raj, K.; Joy, P. A. Ferromagnetism at Room Temperature in Activated Graphene Oxide. *Chem. Phys. Lett.* **2014**, *605-606*, 89−92.
(35) Rao, S. S.; Jammalamadaka, N.; Stesmans, A.; Moshchalkov, V. V.; van Tol, J.; Kosynkin, D. V.; Higginbotham-Duque, A.; Tour, J. M. Ferromagnetism in Graphene Nanoribbons: Split versus Oxidative Unzipped Ribbons. *Nano Lett.* **2012**, *12*, 1210−1217.
(36) Matte, H. S. S. R.; Subrahmanyam, K. S.; Rao, C. N. R. Novel Magnetic Properties of Graphene: Presence of Both Ferromagnetic and Antiferromagnetic Features and Other Aspects. *J. Phys. Chem. C* **2009**, *113*, 9982−9985.
(37) Scheike, T.; Böhlmann, W.; Esquinazi, P.; Barzola-Quiquia, J.; Ballestar, A.; Setzer, A. Can Doping Graphite Trigger Room Temperature Superconductivity? Evidence for Granular High-Temperature Superconductivity in Water-Treated Graphite Powder. *Adv. Mater.* **2012**, *24*, 5826−5831.
(38) Liang, J.; Xu, Y.; Sui, D.; Zhang, L.; Huang, Y.; Ma, Y.; Li, F.; Chen, Y. Flexible, Magnetic, and Electrically Conductive Graphene/Fe_3O_4 Paper and Its Application for Magnetic-Controlled Switched. *J. Phys. Chem. C* **2010**, *114*, 17465−17471.
(39) Ganguly, A.; Sharma, S.; Papakonstantinou, P.; Hamilton, J. Probing the Thermal Deoxygenation of Graphene Oxide Using High-Resolution in Situ X-Ray-Based Spectroscopies. *J. Phys. Chem. C* **2011**, *115*, 17009−17019.
(40) Power, S. R.; Ferreira, M. S. Indirect Exchange and Ruderman-Kittel-Kasuya-Yosida (RKKY) Interactions in Magnetically-Doped Graphene. *Crystals* **2013**, *3*, 49−78.
(41) Ruderman, M. A.; Kittel, C. Indirect Exchange Coupling of Nuclear Magnetic Moments by Conduction Electrons. *Phys. Rev.* **1954**, *96*, 99−102.
(42) Cancado, L. G.; Jorio, A.; Martins Ferreira, E. H.; Stavale, F.; Achete, C. A.; Capaz, R. B.; Moutinho, M. V. O.; Lombardo, A.; Kulmala, T. S.; Ferrari, A. C. Quantifying Defects in Graphene va Raman Spectroscopy at Different Excitation Energies. *Nano Lett.* **2011**, *11*, 3190−3196.
(43) Jorio, A.; Lucchese, M. M.; Stavale, F.; Martins Ferreira, E. H.; Moutinho, M. V. O.; Capaz, R. B.; Achete, C. A. Raman Study of Ion-Induced Defects in N-Layer Graphene. *J. Phys.: Condens. Matter* **2010**, *22*, 334204.
(44) Stankovich, S.; Dikin, D. A.; Piner, R. D.; Kohlhaas, K. A.; Kleinhammes, A.; Jia, Y.; Wu, Y.; Nguyen, S. T.; Ruoff, R. S. Synthesis of Graphene-Based Nanosheets via Chemical Reduction of Exfoliated Graphite Oxide. *Carbon* **2007**, *45*, 1558−1565.

DOI: 10.1021/acs.chemmater.6b04748
Chem. Mater. 2017, 29, 3873−3882

(45) Saito, R.; Jorio, A.; Souza Filho, A. G.; Dresselhaus, G.; Dresselhaus, M. S.; Pimenta, P. A. Probing Phonon Dispersion Relations of Graphite by Double Resonance Raman Scattering. *Phys. Rev. Lett.* **2002**, *88*, 027401.
(46) Park, S.; An, J.; Piner, R. D.; Jung, I.; Yang, D. X.; Velamakanni, A.; Nguyen, S. T.; Ruoff, R. S. Aqueous Suspension and Characterization of Chemically Modified Garphene Sheets. *Chem. Mater.* **2008**, *20*, 6592−6594.
(47) Pisana, S.; Lazzeri, M.; Casiraghi, C.; Novoselov, K. S.; Geim, A. K.; Ferrari, A. C.; Mauri, F. Breakdown of the Adiabatic Born-Oppenheimer Approximation in Graphene. *Nat. Mater.* **2007**, *6*, 198−201.
(48) Ferrari, A. C. Raman Spectroscopy of Graphene and Graphite: Disorder, Electron-Phonon Coupling, Doping and Nonadiabatic Effects. *Solid State Commun.* **2007**, *143*, 47−57.
(49) Sharma, R.; Baik, J. H.; Perera, C. J.; Strano, M. S. Anomalously Large Reactivity of Single Graphene Layers and Edges Toward Electron Transfer Chemistries. *Nano Lett.* **2010**, *10*, 398−405.
(50) Qin, S.; Guo, X.; Cao, Y.; Ni, Z.; Xu, Q. Strong Ferromagnetism of Reduced Graphene Oxide. *Carbon* **2014**, *78*, 559−565.
(51) Lee, C.-L.; Wan, C.-C.; Wang, Y.-Y. Synthesis of Metal Nanoparticles via Self-Regulated Reduction by an Alcohol Surfactant. *Adv. Funct. Mater.* **2001**, *11*, 344−347.
(52) Acik, M.; Lee, G.; Mattevi, C.; Pirkle, A.; Wallace, R. M.; Chhowalla, M.; Cho, K.; Chabal, Y. The Role of Oxygen During Thermal Reduction of Graphene Oxide Studied by Infrared Absorption Spectroscopy. *J. Phys. Chem. C* **2011**, *115*, 19761−19781.
(53) Ogoshi, T.; Ichihara, Y.; Yamagishi, T.-A.; Nakamoto, Y. Supramolecular Polymer Networks from Hybrid between Graphene Oxide and Per-6-Amino-β-Cyclodextrin. *Chem. Commun.* **2010**, *46*, 6087−6089.
(54) Kim, U. J.; Furtado, C. A.; Liu, X.; Chen, G.; Eklund, P. C. Raman and IR Spectroscopy of Chemically Processed Single-Walled Carbon Nanotubes. *J. Am. Chem. Soc.* **2005**, *127*, 15437−15445.
(55) Ciszewski, M.; Mianowski, A. Survey of graphite oxidation methods using oxidizing mixtures in inorganic acids. *CHEMIK* **2013**, *67*, 267−274.
(56) Georgakilas, V.; Otyepka, M.; Bourlinos, A. B.; Chandra, V.; Kim, N.; Kemp, K. C.; Hobza, P.; Zboril, R.; Kim, K. S. Functionalization of Graphene: Covalent and Non- Covalent Approaches, Derivatives and Applications. *Chem. Rev.* **2012**, *112*, 6156−6214.
(57) Raza, M.; Bachinger, A.; Zahn, N.; Kickelbick, G. Interaction and UV-Stability of Various Organic Capping Agents on the Surface of Anatase Nanoparticles. *Materials* **2014**, *7*, 2890−2912.
(58) Shih, C.-J.; Lin, S.; Sharma, R.; Strano, M. S.; Blankschtein, D. Understanding the pH-Dependent Behavior of Graphene Oxide Aqueous Solutions: A Comparative Experimental and Molecular Dynamics Simulation Study. *Langmuir* **2012**, *28*, 235−241.
(59) Konkena, B.; Vasudevan, S. Understanding Aqueous Dispersibility of Graphene Oxide and Reduced Graphene Oxide Through pKa Measurements. *J. Phys. Chem. Lett.* **2012**, *3*, 867−872.

DOI: 10.1021/acs.chemmater.6b04748
Chem. Mater. 2017, 29, 3873−3882